J. Earth Syst. Sci. (2020)129 6
https://doi.org/10.1007/s12040-019-1288-1

Crustal shear-wave velocity structure in Western Java, Indonesia from analysis of teleseismic receiver functions

T Anggono[1,*], S Syuhada[1], F Febriani[1], L Handayani[2], M M Mukti[2] and A Amran[3]

[1] *Research Center for Physics, Indonesian Institute of Sciences, Kawasan PUSPIPTEK, Serpong 15310, Indonesia.*
[2] *Research Center for Geotechnology, Indonesian Institute of Sciences, Kompleks LIPI, JL. Cisitu Sangkuriang, Bandung 40135, Indonesia.*
[3] *Indonesian Agency for Meteorology, Climatology and Geophysics, Jl. Angkasa I, No. 2, Kemayoran, Jakarta 10720, Indonesia.*
**Corresponding author. e-mail: titi.anggono@gmail.com*

MS received 27 June 2018; revised 28 May 2019; accepted 25 August 2019

We analysed receiver functions from teleseismic events recorded at 11 broadband seismometers in the western part of Java Island, Indonesia. The stations are mostly located at three main geological environment including Northwest Java Basin, Bogor Zone, and Southern Mountains Arc. A total of about 341 receiver functions were computed using iterative time domain deconvolution. We derived shear-wave velocity structure and crustal Vp/Vs ratio by inverting stacked radial receiver functions using non-linear neighbourhood algorithm. Inversion results show sediment thickness varies between 1 and 2 km thick in Western Java. Our inversion shows that crustal thickness in this region varies between 25 and 32 km. Average crustal Vp/Vs ratio is estimated to be about 1.69–1.78. We hope the study may provide useful information for velocity model and crustal thickness for Indonesia region.

Keywords. Receiver functions; crustal structure; Moho discontinuity; Western Java.

1. Introduction

Sunda Arc is one of the most seismically active regions in the world. The Sunda Arc curves along the islands of Sumatra and Java with a total length of more than 5600 km starting from Andaman Sea to Sumba Island in Indonesia. It consists Java Trench, forearc ridge, fore-arc basin, and active volcanic arc in Sumatra and Java Islands (e.g., Hamilton 1979; Susilohadi *et al.* 2009). The region has generated several large earthquakes in the last 15 years, such as 2004 Mw 9.1 Sumatra–Andaman, 2005 Mw 8.7 Nias Island, 2006 Mw 7.7 Pangandaran, and 2007 Mw 8.4 South Sumatra. In addition to strong motion, the earthquakes also pose tsunami hazard that may cause large casualty such as 2004 Mw 9.1 Sumatra–Andaman and 2006 Mw 7.7 Pangandaran. Western Java is part of Java Island and the most populous region in Indonesia with a population is of approximately up to 50 million. In addition to the earthquakes from Sumatra–Andaman subduction zone, the region also consists of Cimandiri fault zone, which encompasses Cimandiri fault and a series of other smaller faults. The Cimandiri fault zone is approximately 100 km long with trends from the south coast to the western part of Bandung (Darji *et al.* 1994; Malod *et al.* 1995; Abidin *et al.* 2009; Susilohadi *et al.* 2009). Damaging earthquakes have occurred close to the proximity and are

Published online: 19 December 2019

thought to be attributed to this fault zone, such as M5.5 1982, M5.5, M5.1 Sukabumi earthquakes in 2000, and numerous M5–6 earthquakes since 1629 (Marliyani *et al.* 2016).

A number of studies have been carried out to investigate geodynamic, tectonic evolution and crustal structure offshore Western Java using seismic reflection (e.g., Kopp *et al.* 2002, 2009; Schlüter *et al.* 2002), refraction and gravity data (Kopp *et al.* 2001, 2002). However, information on crustal structure onshore Western Java is still less studied, which is very important for understanding the evolution of Java Island. Contradict to Western Java; several studies have been carried out to investigate deep crustal structure in Central using data from a temporary network of MERAMEX (e.g., Koulakov *et al.* 2007, 2009; Zulfakriza *et al.* 2014; Wölbern and Rümpker 2016). It has been suggested that Western Java is separated from Central and East Java by Meratus suture (Smyth *et al.* 2007; Clements and Hall 2011; Hall 2012). Meratus suture may indicate a differentiation of crustal origin of Central-East Java, which might come from Banda block, and Western Java that might come from Sunda block. For Sumatra region, which is part of Sunda block, several studies have been carried out to determine crustal structure Sumatra using seismic reflection (e.g., Kopp *et al.* 2001; Franke *et al.* 2008; Singh *et al.* 2008), receiver functions (e.g., Kieling *et al.* 2011; Macpherson *et al.* 2012; Bora *et al.* 2016) or ambient noise analysis (Harmon *et al.* 2012).

One method to obtain Earth's structure information is receiver function analysis, which uses teleseismic events. The method is robust for estimating crustal properties beneath seismic stations (e.g., Chevrot and van der Hilst 2000; Crotwell and Owens 2005). Arrival time of *Ps*, *PpPs* and *PpSs*+*PsPs* converted and reverberated phases from Moho interface can be combined to constrain in determining crustal thickness and *Vp*/*Vs* ratio. Zhu and Kanamori (2000) applied receiver function analysis to estimate the Moho depth variation and Poisson's ratio in Southern California, USA. Ahmed *et al.* (2014) imaged crustal thickness variation from computed receiver function in the eastern Gulf of Aden continental margins. Recent studies in the Sunda arc region applied receiver function analysis, for example Macpherson *et al.* (2012) and Bora *et al.* (2016) investigated crustal structure in Sumatra Island, and Wölbern and Rümpker (2016) crustal thickness in Central and East Java using temporary network of MERAMEX. It was suggested that crustal thickness to be about 16 km in the forearc and up to 35 km at the backarc basin of Sumatra Island (Macpherson *et al.* 2012; Bora *et al.* 2016). Bai *et al.* (2010) carried out receiver function analysis in Vietnam, which is part of Sunda block. They found the crustal thickness ranges between 29 and 45 km. Wölbern and Rümpker (2016) investigated crustal thickness in Central and East Java from receiver function analysis and obtained an average crustal thickness of about 34 km. In recent years, the installation of seismic broadband stations in western part of Java Island may enable us to study crustal structure through receiver function method for the broader scale coverage of Western Java. In this study, we applied receiver function analysis to determine the regional variation of the crustal properties in the Western Java.

2. Geological setting

Java Island is located between Eurasia and Australia, on the southeast margin of Eurasian plate. The southeastern part of the Eurasian plate is also called Sunda block, which is a Mesozoic continental core of southeast Asia (Hamilton 1979; Smyth *et al.* 2007). During the late Cretaceous, terranes of arc and ophiolitic materials were accreted to the southern margin of Sunda block along a northeast–southwest trending subduction zone. Subduction moved to its present-day location and east–west orientation along the Java trench in Early Paleogene (Hall 2012; Smyth *et al.* 2007). Width and location of interpreted NE–SW orientation of the Cretaceous subduction zone or Meratus suture are not well constrained and differ in previous studies (e.g., Wakita 2000; Smyth *et al.* 2007; Clements and Hall 2011). Australian plate subducts beneath Sunda block at the Java Trench in an almost perpendicular direction to the trench off the south coast of Java Island and at an oblique angle off the west coast of Sumatra Island, Indonesia. Currently, the subduction rate gradually decreases from 68 mm/yr off central Java to 60 mm/yr off central Sumatra (DeMets *et al.* 2010). The collision of India and Eurasia caused massive amount of sediments to be formed into the Indian Ocean and the Java Trench, rapidly accreted and creates large accretionary prism (Susilohadi *et al.* 2009). According to van Bemmelen (1949), the main structural elements of Java Island are the geanticline, a broad uplift of regional extend in south Java extending along the southern half of the island, and the geosynclinals basin of north Java occupying its northern half. The southern flank of the Java-geanticline is formed by the Southern Mountains. The Southern Mountains consist of volcanic deposits of the old-andesites formed in the Miocene age. Bogor-North Serayu-Kendeng Zone is located directly north of Southern Mountains and oriented parallel to with EW orientation. The Kendeng Zone was filled with volcanoclastic materials and sediments are suggested up to 8 km thick (De Genevraye and Samuel 1972; Sujanto and Sumantri 1977). Basement character beneath Java Island is still unknown and exposures of basement rocks in the Island are rare. In Western Java, exposure of basement rock can only be found in Ciletuh. Pre-Tertiary Ciletuh complex, is an NE–SW trending assemblage of rocks comprising serpentinized ultramafics with partially amphibolitized gabro dykes, pillow basalt, volanic breccia, hyaloclastite and greywacke (Parkinson *et al.* 1998). Due to its tectonic activity, Java Island has a series of large-scale structural lineations that have been identified by several studies. These have two distinct orientations; NE orientated structures thought to be related to NW directed subduction during the Cretaceous and EW structures that are more recent and are related to the current subduction system (Simons *et al.* 2007; Clements *et al.* 2009). Examples of the NE and EW orientated structures include Cimandiri Fault Zone and Lemba (figure 1).

3. Data and method

Receiver function method has been used extensively to estimate crustal properties (e.g., Langston 1979; Ammon *et al.* 1990; Chang and Baag 2005; Park *et al.* 2009). Receiver function exploits the information contained from the observation of P to S conversion generated at the Moho, or other interface within the crust, from teleseismic events. The recorded arrival P wave may contain information on the earthquake source, earth structure and the propagation effect (Cassidy 1992; Park *et al.* 2009). By removing the effect of earthquake source and propagation effect, it may be possible to extract information on the earth structure beneath a station. The computed receiver functions consist of converted phases associated with the seismic discontinuities, such as Moho. The procedure is to deconvolve the vertical component from the radial and transverse components in either time or frequency domain to retrieve signals related to the crustal structure (Langston 1979; Ammon 1991).

We analysed seismograms from teleseismic events from 2007 to 2013 recorded at 11 permanent broadband seismometers of GE and IA-network located in Western Java, Indonesia. The seismometers cover relatively diverse geologic environment (figure 1). We selected teleseismic events with distances between 30° and 90°. The criterion was selected to avoid contamination from regional phases and to assure that incoming waves have steep incident. We selected events with magnitudes larger than 5.5 to obtain waveforms with good signal to noise ratio. The events are selected based on the International Seismological Commission catalogue (ISC 2013). We manually inspected the data to select good quality of the recorded seismograms and applied instrument correction. The horizontal components of the seismograms were rotated into radial-transverse components. Then, we selected the time window of −10 s before and 50 s after the P-wave arrival.

We computed receiver functions using iterative deconvolution method (Ligorria and Ammon 1999). Iterative deconvolution calculates the receiver functions by minimizing the difference between observed horizontal component and synthetic receiver function from the convolution of the observed vertical component and an iteratively updated spike train (Ligorria and Ammon 1999). The iterative deconvolution may reduce acausal noise significantly compared to the receiver functions calculated using water level frequency domain deconvolution (Ligorria and Ammon 1999; Macpherson *et al.* 2012). We compared receiver functions from a teleseismic earthquake computed using iterative and water level frequency domain deconvolution at station CGJI (figure 2). Those receiver functions were computed by applying Gaussian filter with a width parameter of 1.5. Gaussian filter was applied to reduce high frequency noise in the calculated receiver function. Gaussian filter width parameter of 1.5 may correspond to low pass filter with a corner frequency of 0.75 Hz. The value was chosen after trial and error to find good quality of receiver functions. The iteration was limited to 500 iterations, with both radial and transverse components were calculated. A misfit, which was

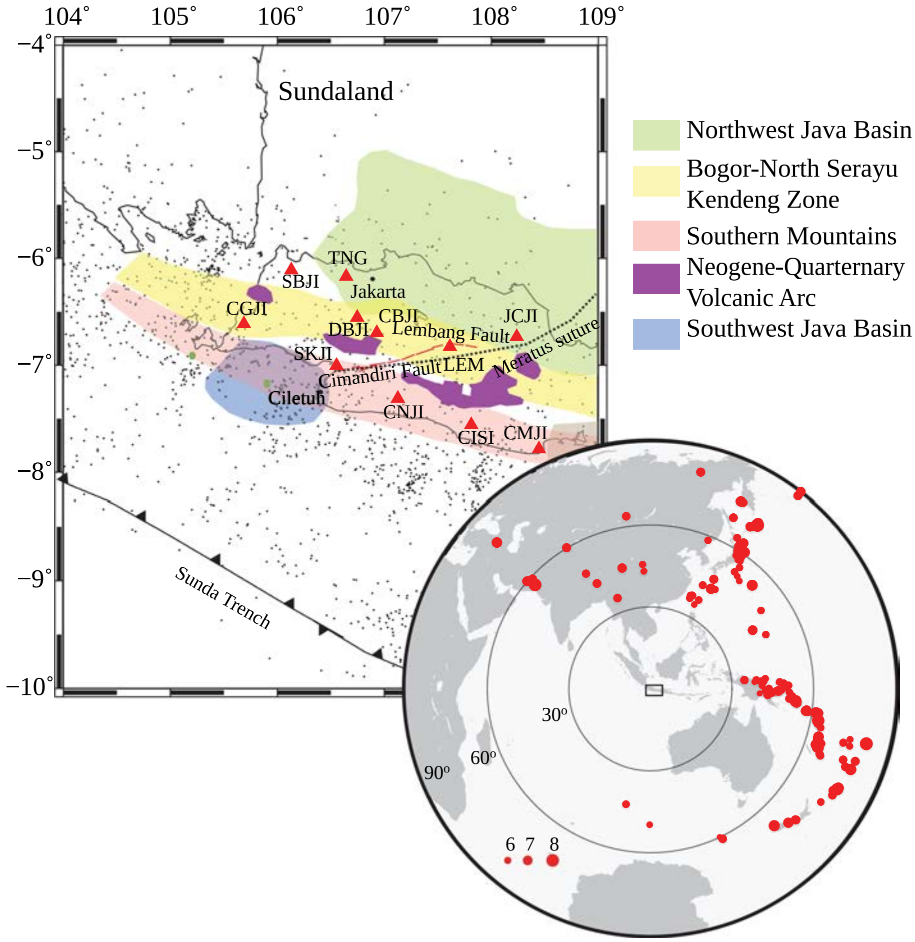

Figure 1. Geological setting of the study area shows location of the broadband seismometers installed (solid red triangles) in Western Java used in this study. Dashed red lines represent estimated location of Cimandiri and Lembang Fault. Black line represent estimated location of Meratus suture. Small black circles represent the earthquake epicentres in this region. The globe shows distribution of the teleseismic events used in this study with their magnitude scales (solid red circles). The solid black square represents the study area on the larger map.

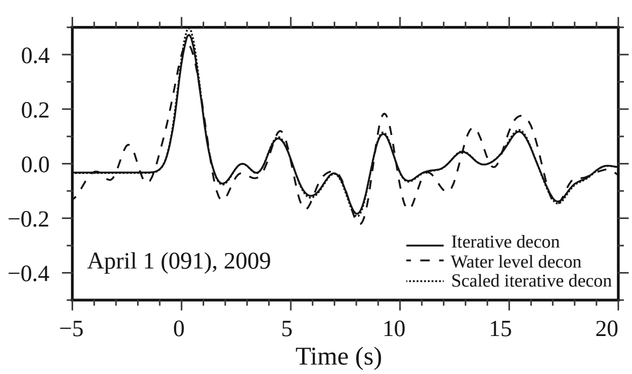

Figure 2. Computed receiver functions at station CGJI from a teleseismic earthquake with an iterative deconvolution (solid line), water level frequency domain deconvolution (dashed line), and scaled iterative deconvolution (dotted line). Scaled iterative deconvolution is receiver function computed using iterative deconvolution and divided by 0.85 for Gaussian filter with width parameter of 1.5.

calculated from the difference between the observed and calculated receiver functions, was used to assess the quality of the calculated receiver functions. We selected radial receiver functions with at least 85% fit for further analyses. We computed about 341 receiver functions from teleseismic events, which mostly are from N–NE and E–SE directions. In an isotropic homogeneous medium, transverse receiver function shows no energy. Occurrence of energy in the transverse receiver function might be due to presence of lateral heterogeneity such as dipping layers or anisotropy (e.g., Savage 1998; Bianchi *et al.* 2015; Bora *et al.* 2016). We grouped computed receiver functions with similar back azimuth and then stacked them. Back azimuths were selected based on the distribution of the data and waveform similarity, which are at 20°–45°, 50°–75°, 80°–105°, 105°–130°, and 310°–335°. Due to lack of azimuthal coverage of available events, we could not discuss on the possible effect of heterogeneity in this study through receiver function modelling. In this study, we focussed on the estimation of lithospheric structure from the radial receiver functions.

Receiver function is nonlinearly sensitive to the subsurface *S*-wave velocity, so that it provides information on the *S*-wave velocity structure. The *S*-wave velocity structure derived from linearized inversion can be dependent on the initial velocity model. In this study, we investigated the *S*-wave velocity profile beneath the stations from the computed receiver functions using nonlinear nearest-neigbourhood inversion algorithm (NA) of Sambridge (1999a, b). The method uses randomized or stochastic sampling to search for solutions with acceptable data fit, which is similar to Genetic algorithm (GA). On GA, the information obtained from the previous samples is highly dependent on the control parameters. The NA differs in requiring only two control parameters to be tuned and the search progress is lead by the models rank with respect to the data misfit criterion. Studies has been carried out using NA inversion to estimate crustal structure from receiver function observations (e.g., Bannister *et al.* 2003, 2004; Hetényi and Bus 2007; Lodge *et al.* 2012). Sambridge (1999a) suggested that NA may be capable of estimating the depth and velocity jump or discontinuity across the Moho quite well and better at the basement layer compared to that than GA applied by Shibutani *et al.* (1996). Shibutani *et al.* (1996) suggested that the inverted velocity from receiver functions might differ with true velocity for about 4% in the shallower part (<3 km) and greater depths (>20 km), but about 10% at middle depths (3–20 km). NA algorithm uses stochastic sampling to search optimum model in the range of acceptable velocity models. In this technique, the structure is divided into six layers; sediment, basement, upper, middle, lower crust, and upper mantle. In each layer, four parameters are parameterized by describing layer thickness (km), *S*-wave velocity at the top and bottom layers (km/s), and Vp/Vs ratio. We tested reliability of the NA inversion using one-dimensional velocity model consists of sedimentray layer (~1 km), basement (~3 km), upper (~10 km), middle (~14 km), lower crust (~12 km) and upper mantle (halfspace). We generated synthetic three component seismograms from a teleseismic earthquake and computed receiver functions using iterative deconvolution and water-level frequency domain deconvolution. Receiver functions were computed using Gaussian filter with width parameter of 1.5. We also scaled the obtained receiver function from iterative deconvolution by dividing it with 0.85 (figure 3a–d). We also introduced other models for the comparison of NA inversion, which are velocity decrease at crustal and upper mantle, sharp velocity contrast, and low velocity at middle crust (figure 3e–g). From these results, we suggest that NA inversion from the computed receiver functions are able to extract information about layer thickness and shear wave velocity (Vs). In this study, we selected Gaussian filter with width parameter of 1.5 corresponding to low pass filter of ~0.75 Hz. By assuming average crustal shear wave velocity of 3.6 km/s, the corresponding wavelength (λ) is about 4.8 km. By considering the vertical resolution might be resolvable to about λ/4, we suggest that the resolvable layer thickness is about ~1.2 km. Our modeling shows that by using Gaussian filter with width parameter of 1.5, we are able to resolve sedimentary layer thickness down to about 1 km thick.

To perform the NA inversion, we set initial model as follows: sediment layer consists of layer thickness of 0–2 km, *S*-wave velocities at top and bottom of 0.5–2.0 and 0.5–2.0 km/s and Vp/Vs ratio of 2.0–3.0. Basement layer is set with layer thickness of 0–3 km, *S*-wave velocities at top and bottom of 1.3–3.3 and 1.3–3.3 km/s and Vp/Vs ratio of 1.65–2.5. Upper crust is set with layer thickness of 0–15 km, *S*-wave velocities at top and bottom of 2.4–3.6 and 2.4–3.9 km/s and Vp/Vs ratio of 1.65–1.90. Middle crust is set with layer thickness of 5–15 km, *S*-wave velocities at top and bottom of 3.0–4.2 and 3.4–4.2 km/s and Vp/Vs ratio of 1.65–1.9. Lower crust is set with layer thickness of 5–15 km, *S*-wave velocities at top and bottom of 3.0–4.5 and 3.4–4.5 km/s and Vp/Vs ratio of 1.65–1.9. And upper mantle is set with layer thickness of 5–30 km, *S*-wave velocities at top and bottom are 4.0–5.0 and 4.0–5.0 km/s and Vp/Vs ratio of 1.7–1.9. NA inversion is applied to the stacked receiver functions. The stacked receiver function is obtained by stacking receiver functions with similar back azimuth so that it can enhance the main signal as well as to reduce the 3-D effects due to lateral variation and to provide average

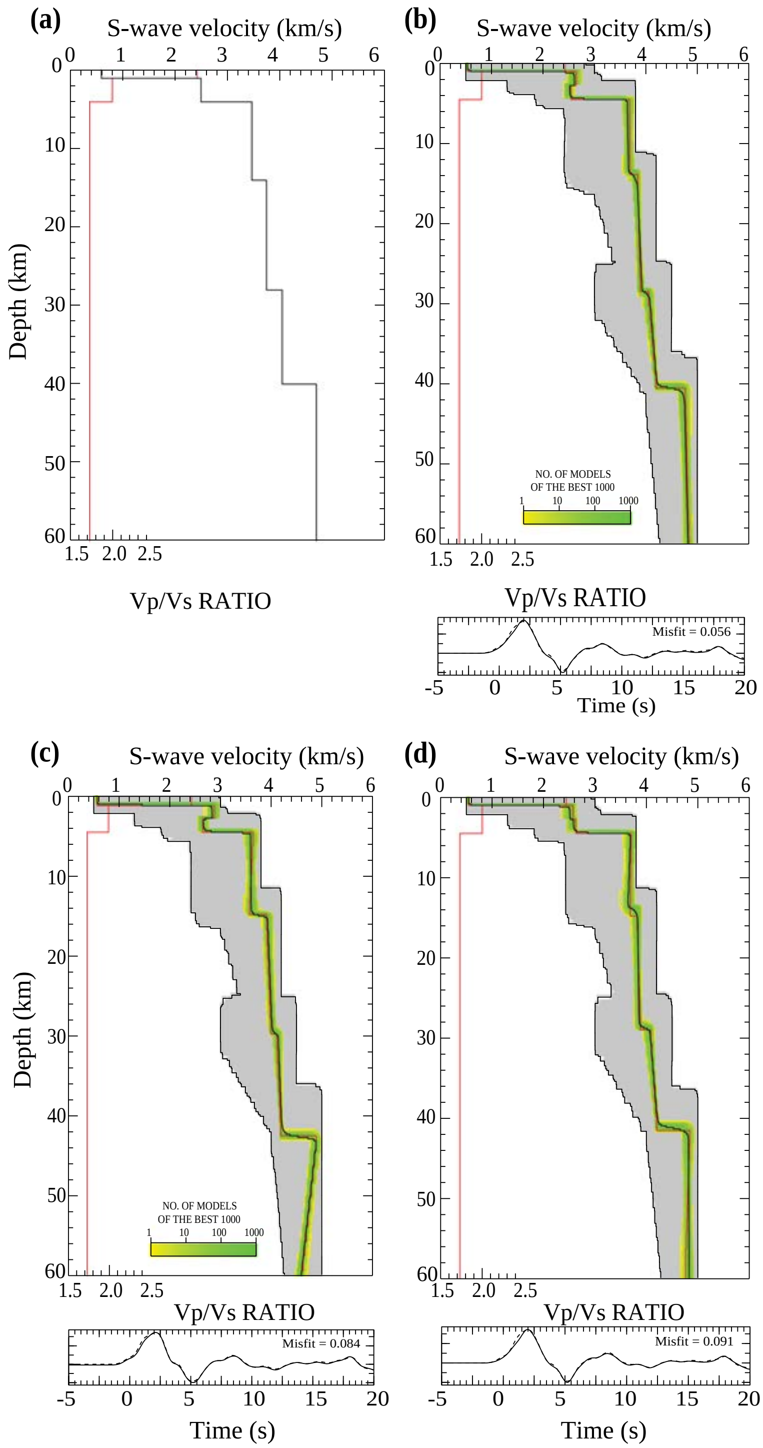

Figure 3. Test of NA inversion result from computed receiver functions. **(a)** Gradual velocity increase model beneath a station. **(b)** NA inversion result from computed receiver function using iterative deconvolution (top panel) with red and black lines show the best fit and average of *Vs*, with red line in the left upper panel shows the best fit of *Vp*/ *Vs*. At the bottom panel, solid and dashed lines show observed and synthetic receiver functions, respectively. **(c)** Same as (b) but for computed receiver function using water-level deconvolution. **(d)** Same as (b) but receiver function was divided by 0.85. **(e–g)** Models consist of velocity decrease in crustal and upper mantle, sharp velocity contrast and low velocity of middle crust (left panels) and their NA inversion results (right panels).

crustal model (Zhu and Kanamori 2000). We chose time window of –5 s and 20 s after direct P arrival for the inversion process. The time window was chosen by assuming that the all converted phases were included. We set the inversion for 5000 iterations, providing about 250,050 velocity models.

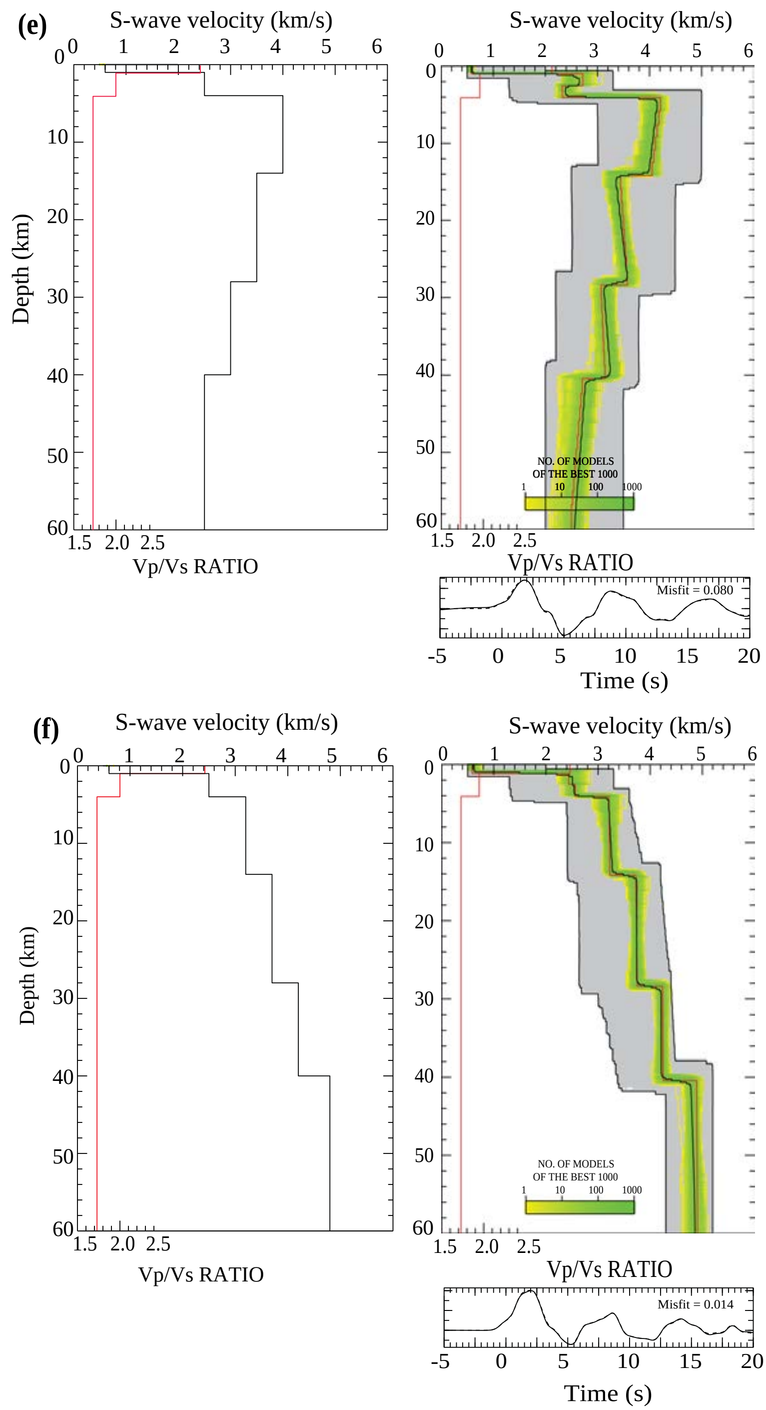

Figure 3. *(Continued.)*

4. Results and discussion

4.1 *Northwest Java Basin*

First we examined calculated receiver function at station JCJI and TNG located on the Northwest Java Basin (figure 4). Similar characteristics of radial receiver functions are observed at both stations. The receiver functions are complex in the first 0–3 s. The initial phases at around 0 s show relatively broad or large amplitudes. We suggest that this could be due to the presence of thick deposit of low velocity sediments. The low velocity sediment may cause a *Ps* converted phase from the bottom of the sediment (Bannister *et al.* 2003). The composition between the *Ps* and direct *P* phases may cause such broad amplitude and produce a shifted peak from 0 s. Addition to the composition

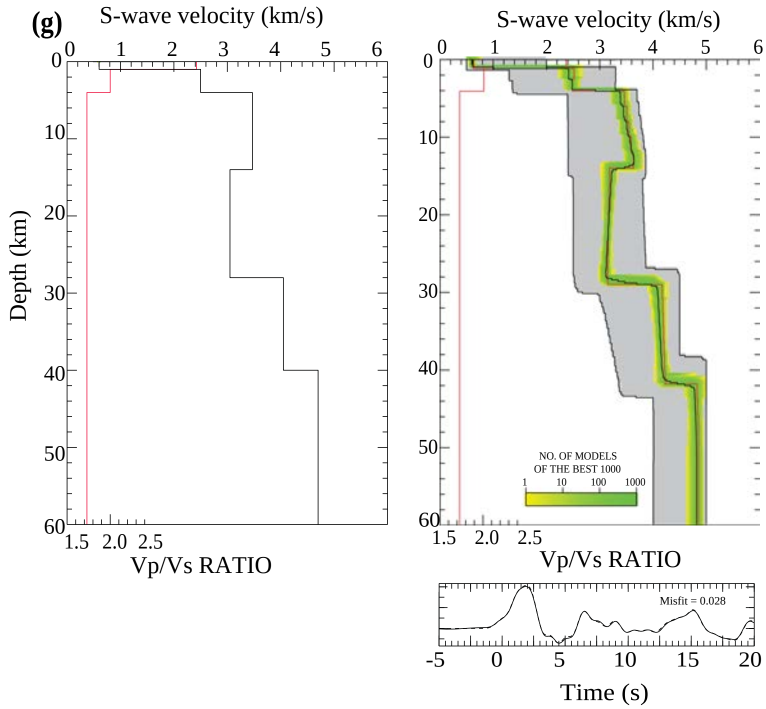

Figure 3. *(Continued.)*

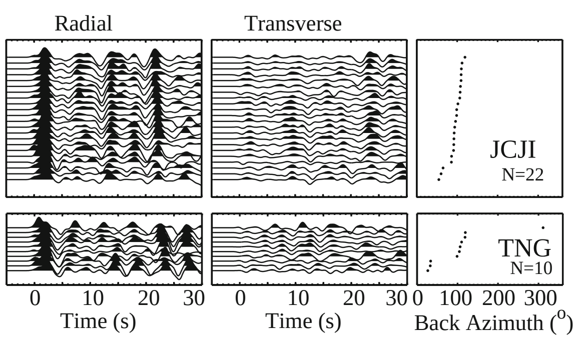

Figure 4. Observed receiver functions at stations located in Northwest Java Basin. Receiver functions are plotted with equal spacing as a function of back azimuth. Positive arrivals are depicted as solid black. *N* corresponds to the number of receiver functions.

of these phases, reverberation inside the sedimentary layers may contribute to the complexity around the direct *P* phase arrival. Several studies have shown similar characteristics at shallow sedimentary basins (e.g., Sheehan *et al.* 1995; Shibutani *et al.* 1996; Clithore *et al.* 2000). It is also shown that shape of the pulse in the first 3 s for observed radial receiver functions varies with back azimuth.

For back azimuth between 20° and 120°, radial receiver functions for stations JCJI and TNG show similar characteristics in the first 3 s, with weak pulse of direct *P*-phases followed by strong pulse around 2–3 s. At back azimuth of 310°, strong pulse of direct *P*-phase is observed at station TNG. Bannister *et al.* (2003) suggested that changes in observed receiver functions with back azimuth may indicate lateral changes in the sedimentary thickness, sedimentary velocities or basement conditions near the station. We suggest similar characteristics of sedimentary effect can be found in Northwest Java basin as sedimentary thickness and geometry varies in this basin (Noble *et al.* 1997; Bishop 2000).

We searched *S*-wave velocity model using non-linear neighbourhood inversion technique of Sambridge (1999a, b). Figure 5 shows density plots of the *S*-wave velocity model generated from the inversion. We plotted 1000 best models and the lateral bound of how well the velocity structure is constrained. From the calculated models, we obtained best fitting model that generates the least misfit between the calculated and observed receiver functions (figure 5). Theoretical receiver function was calculated from the best fitting model from the inversion to see the waveform comparison with the observed receiver function.

Crustal structure beneath station JCJI is estimated from the inversion of stacked receiver functions from three different back azimuths. Inversion result from receiver functions in 50°–75° shows about 2 km thick of sediment layer with

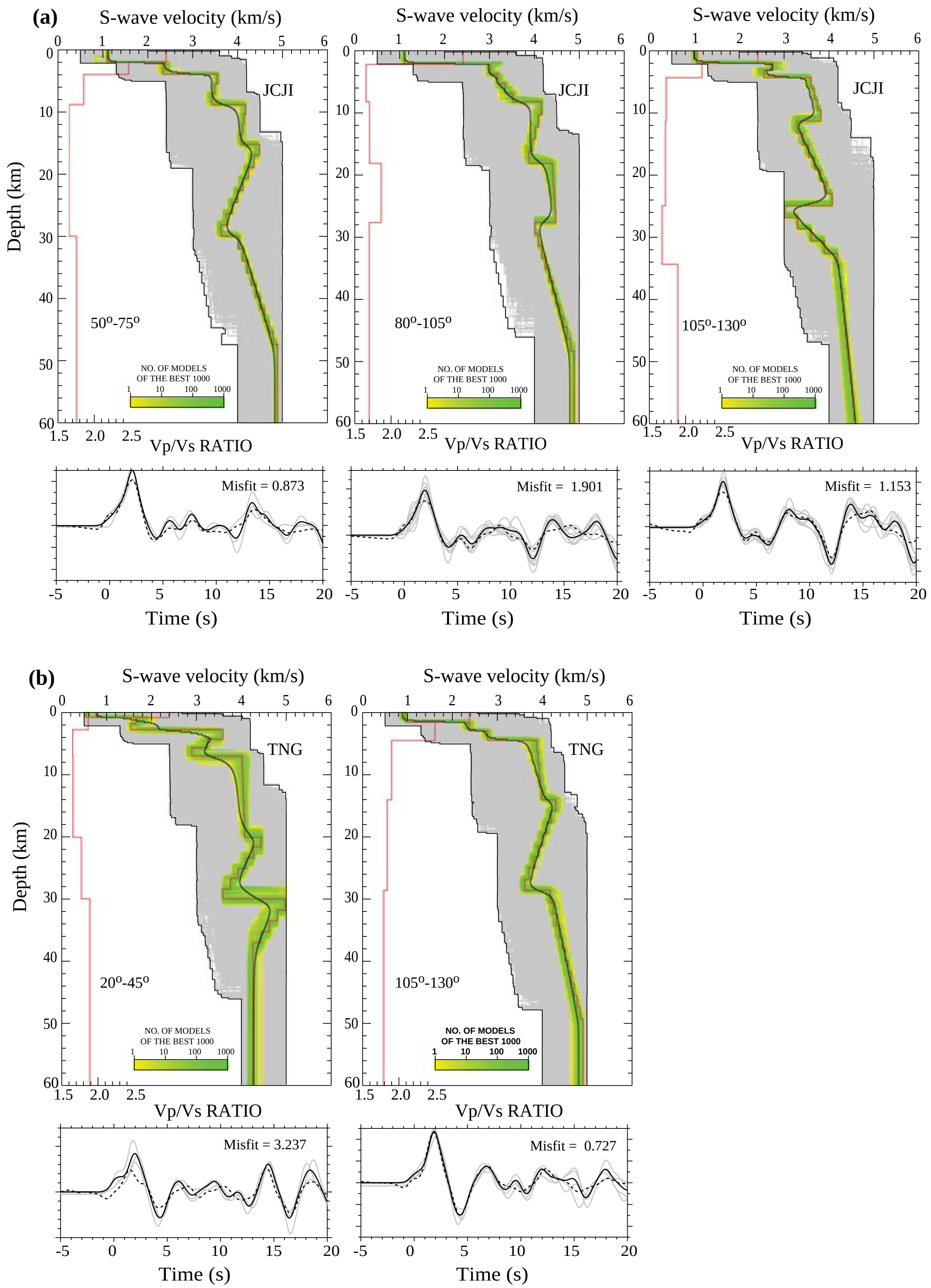

Figure 5. Derived *S*-wave velocity model for stations **(a)** JCJI and **(b)** TNG located in the Northwest Java Basin (upper panel) for each back azimuth direction. All 250,050 models searched in the inversion are outlined by light-grey shaded area. The green shaded regions indicate the density of 1000 best models. The solid red and black lines represents the best model and average of the best 1000 models *Vs* model. The solid red line on the left upper panel represents the best fitting *Vp*/ *Vs* ratio. Lower panel shows synthetic radial receiver functions (dashed line) using the best fitting *S*-wave velocity model from the nonlinear inversion, together with the observed stacked and individual radial receiver functions (solid black and grey lines).

Table 1. *Inversion results for sediment thickness (H^s), sediment shear wave velocity (Vs^s), sediment Vp/Vs ratio (Vp/Vs^s), crustal thickness (H^c), average crustal shear wave velocity (Vs^c), crustal Vp/Vs ratio (Vp/Vs^c) and Moho depth estimated from stacked receiver functions in narrow back azimuth ranges (BAZ).*

Station code	BAZ (°)	N	H^s (km)	Vs^s (km/s)	Vp/Vs^s	H^c (km)	Vs^c (km/s)	Vp/Vs^c	Moho depth (km)
JCJI	50–75	3	2	1.11	3.00	24	3.86	1.72	30
	80–105	11	2	1.11	2.99	24	3.92	1.74	28
	105–130	8	2	1.00	2.99	28	3.74	1.71	34
TNG	20–45	3	1	1.00	2.98	27	3.69	1.70	30
	105–130	4	1	1.00	2.97	23	3.65	1.80	29
CGJI	20–45	5	1	1.28	2.63	33	3.42	1.81	38
	80–105	8	1	1.68	2.36	33	3.51	1.75	34
	105–130	9	1	1.29	2.29	29	3.42	1.75	31
	80–160	19	1	1.58	2.02	30	3.50	1.75	33
CBJI	20–45	4	2	1.43	2.99	28	3.39	1.90	33
	80–105	16	1	1.80	2.37	29	3.59	1.67	33
	105–130	6	1	1.60	2.00	33	3.58	1.69	37
DBJI	80–105	6	2	1.71	2.22	30	3.63	1.72	37
LEM	20–45	20	1	1.91	2.53	30	3.19	1.68	32
	50–75	3	1	1.84	2.90	30	3.13	1.65	32
	80–105	29	1	1.97	2.28	32	3.55	1.67	34
	105–130	10	2	1.46	2.02	31	3.50	1.77	37
	80–110	34	2	1.56	2.05	29	3.45	1.66	32
CNJI	20–45	6	1	1.26	2.85	23	3.70	1.89	25
	80–105	7	1	1.67	2.52	24	3.76	1.70	26
	105–130	6	1	1.28	2.28	28	3.62	1.67	32
	50–130	15	1	1.50	2.99	28	3.71	1.84	31
CISI	20–45	24	1	1.60	2.54	32	3.29	1.86	34
	80–105	27	1	1.51	2.99	24	3.82	1.71	26
	105–130	13	1	1.70	2.05	26	3.85	1.71	29
	310–335	4	1	1.81	2.90	27	3.52	1.76	32
	50–160	45	1	1.68	2.07	26	3.89	1.69	28
CMJI	20–45	8	2	1.66	2.91	34	3.44	1.72	37
	80–105	13	1	1.49	2.97	31	3.78	1.75	35
	105–130	8	1	1.88	2.99	32	3.68	1.86	34
	80–130	21	1	1.76	2.99	30	3.57	1.78	33
SKJI	20–45	7	1	1.37	2.55	30	3.38	1.84	33
	80–105	9	2	1.57	2.90	24	3.45	1.73	29
	105–130	9	1	1.98	2.38	32	3.61	1.78	34
	310–335	4	1	1.00	2.91	32	3.62	1.69	36
SBJI	105–130	9	1	0.98	2.96	28	3.72	1.70	30

N represents number of receiver functions used for stacking.

shear wave velocity (Vs^s) of about 1.11 km/s. It is followed by increase of Vs of about 3.30 km/s at depth of about 4 km and then Vs continue to increase of about 4.2 km/s at depth of about 16 km and decreases. Crustal thickness, average crustal Vs (Vs^c) and crustal Vp/Vs (Vp/Vs^c) is estimated to be about 24 km, 3.86 km/s, and 1.72, respectively. Inversion results for back azimuth 80°–105° show about 2 km thick of sediment layer with Vs^s $\sim$1.1 km/s ($Vp/Vs^s = 2.99$). Crustal thickness is estimated at about 24 km, with average crustal Vs^c of 3.92 km/s ($Vp/Vs^c = 1.74$). For back azimuth 105°–130°, inversion results show about 2 km thick of sediment layer with $Vs^s = 1.00$ km/s ($Vp/Vs^s = 2.99$). Vs of about 4.0 km/s, which represent mantle velocity is observed at depth of 34 km. Crustal thickness, average crustal shear wave velocity Vs^c and Vp/Vs^c are estimated to be about 28 km, 3.74 km/s and 1.71, respectively. At station TNG, crustal structure is estimated from the inversion of stacked receiver functions from two different back azimuths. Inversion from back azimuth 20°–45° shows S-wave low velocity of about 1.0 km/s in the near surface down to about 1 km

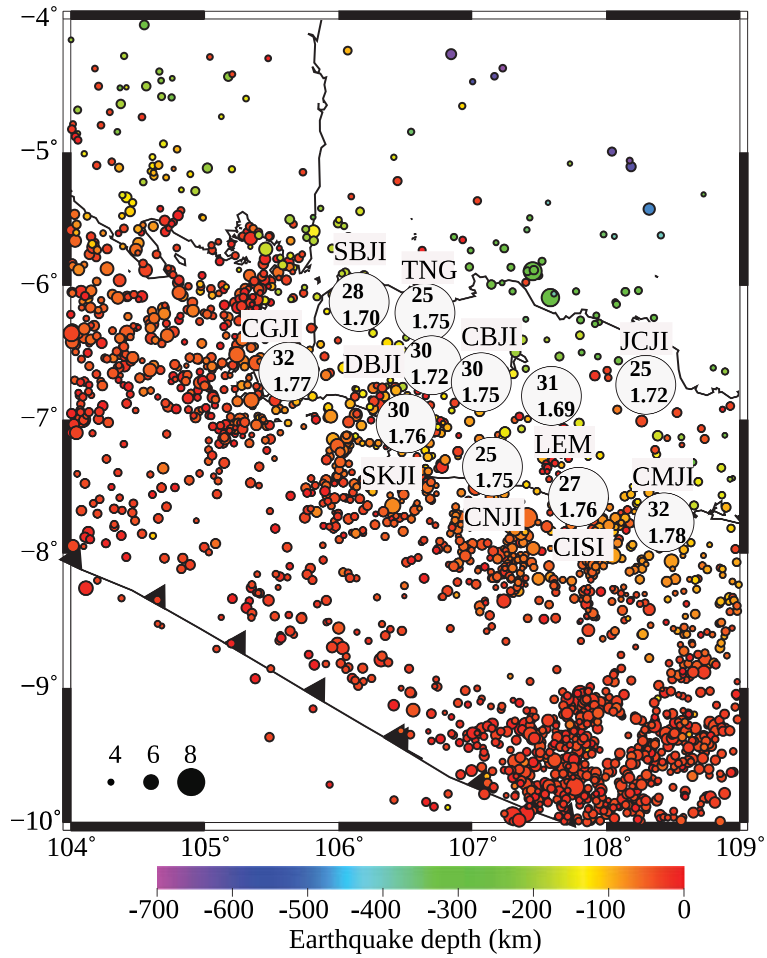

Figure 6. Average crustal thickness and Vp/Vs ratio (inside open circles) estimated from the inversion of receiver functions. Earthquakes in Western Java are shown in solid circles with color representing its depth.

suggesting the presence of thick sediment beneath the station. Crustal thickness, average crustal shear wave velocity Vs^c and Vp/Vs^c are estimated to be about 23–27 km, 3.65–3.69 km/s and 1.70–1.80. The crustal thickness beneath stations located in the Northwest Java Basin is about ∼23 to 28 km. In figure 1, the region of Northwest Java Basin is part of the Sunda block. We suggest that the typical crustal thickness in this region should be comparable to the crustal thickness in Sumatra Island, which is also part of Sunda block, of about up to 35 km depth in the backarc (Bai *et al.* 2010; Macpherson *et al.* 2012; Bora *et al.* 2016). The obtained Vp/Vs ratio of 1.70–1.80 is also consistent with the obtained Vp/Vs ratio by Bora *et al.* (2016) in Sumatra Island. The Vp/Vs ratio represents average crustal composition and may depend on the lithology, temperature, cracks or pore fluid (Fountain and Christensen 1989; Zandt and Ammon 1995). Christensen (1996) classified the typical value of Vp/Vs for various types; for example, felsic rocks (∼1.70), intermediate rocks (∼1.8) and mafic rocks (∼1.84). Table 1 and figure 6 show summary of our receiver function inversion carried out in Western Java.

Northwest Java Basin, which is a back arc system located between Sunda micro Plate and India–Australian Plate, consists of several sub-basins (e.g., Suyitno and Yahya 1974; Adnan *et al.* 1991). The observation stations JCJI and TNG are located in the Jatibarang and Ciputat sub-basins, respectively. Tectonic activities in this regions caused formation of the N–S trending normal fault to the north of the basin. These faults controlled horst and graben structures that influenced sediment in the Northwest Java Basin. Geomorphologically, the area has a low topography and most of the area is covered by alluvial and volcanic products except in the southernmost part of the central area. Sediments were basically from the eroded emergent Sunda shelf entering the basin from the north direction. The Northwest Java

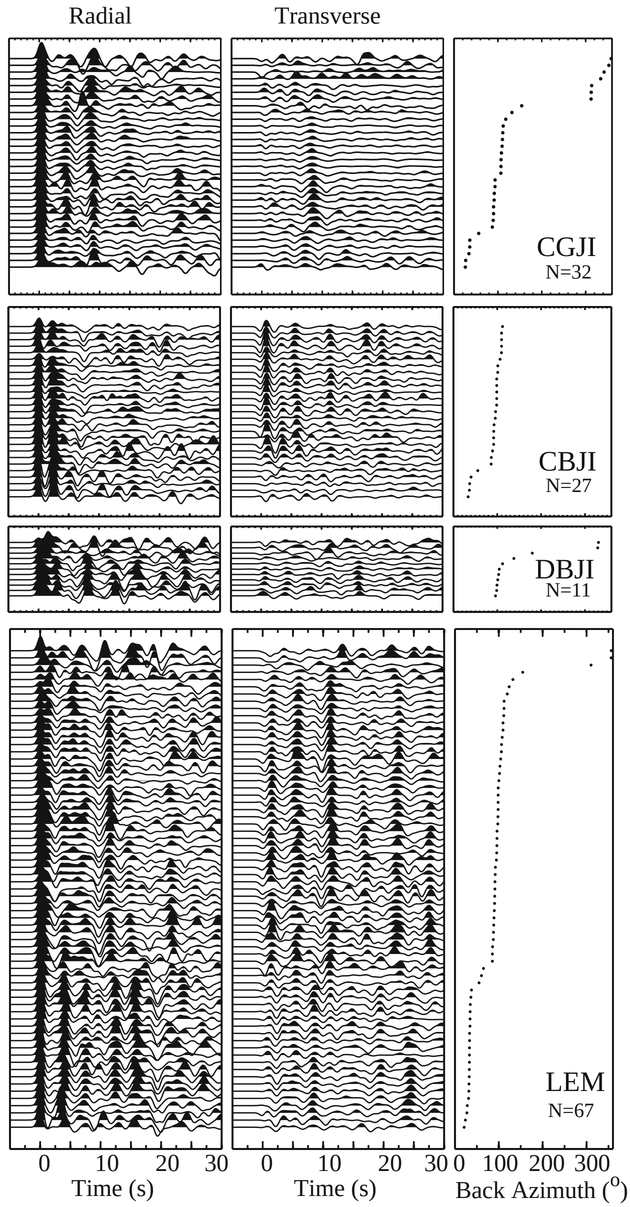

Figure 7. Observed receiver functions at stations located in Bogor-North Serayu-Kendeng Zone.

Basin consists of thick tertiary sediment estimated to be more than 3.0 km thick (Patmosukismo and Yahya 1974; Adnan *et al.* 1991; Bishop 2000). Saygin *et al.* (2016) inverted shear wave structure in Jakarta region, which is part of Northwest Java Basin, and suggested sediment thickness of up to about 1.5 km. Their results are consistent with our analysis using receiver function, which we suggest to be about 1–2 km thick.

4.2 *Bogor Zone*

Figure 7 shows observed radial and transverse receiver functions for stations located in Bogor Zone. At station CGJI, direct *P*- phase is generally observed around 0 s. However, for back azimuth between 20° and 30° direct *P* phase is shifted about 0.5 s. For back azimuth of 150°–160°, we observed broad amplitudes of direct *P* phase. *Ps* phases are generally observed at around 4.0–4.5 s. Clear *Ps* phase is observed for back azimuth of 60°–320°, and less clear *Ps* phase at back azimuth 20°–40°. At station CBJI, we observe two large amplitudes in the first 3 s. Strong pulse with amplitude similar with direct *P* phase appears about 2 s after direct *P* phase. Bannister *et al.* (2003) carried out numerical calculation of sediment effect on the radial receiver function. They observed that the first few seconds of receiver function becomes complex due to reverberation of incoming waves within sediment layer. At station DBJI, complex waveform of radial receiver functions are observed at 0–5.0 s. Similar characteristics of broad amplitudes and complex waveforms in the first few seconds are also observed at stations JCJI and TNG, which we suggest the complexity due to the presence of low velocity layers near the surface. At stations LEM, direct *P* phase show a relatively less complex waveform compared to that of station CBJI. A complex waveform is observed for back azimuth 90°–340°. However, we could observe clear arrival of direct *P* phase for back azimuth 20°–70° and followed by second pulse at 3–4 s. We suggest that at this direction, sedimentation layer has little effect at the calculated receiver functions. The *Ps* phase at station LEM is estimated at about 4–5 s.

S-wave velocity model inversion for stations in Bogor-North Serayu-Kendeng Zone are shown in figure 8. Inversion results for station CGJI for a back azimuth 20°–45° indicate a sedimentary layer of about 1 km thick and increase shear wave velocity indicating Moho interface at depth of about 36–38 km. At back azimuths 80°–105° and 105°–130° also show low velocity layer near the surface down to depth of about 1 km. Moho interface is quite well defined at about 32–34 km depth. Average crustal thickness H^c, shear wave velocity Vs^c and Vp/Vs^c are estimated about 29–33 km, 3.42–3.51 km/s, and 1.75–1.81, respectively. We also stacked receiver functions at broader back azimuth of 80°–160°, and we obtained that the crustal thickness H^c, shear wave velocity Vs^c and Vp/Vs^c are about 30 km, 3.50 km/s, and 1.75, respectively. At station CBJI, crustal structure can be derived from stack receiver functions from three different back azimuths. We obtained low velocity layer of about 1–2 km thick near the

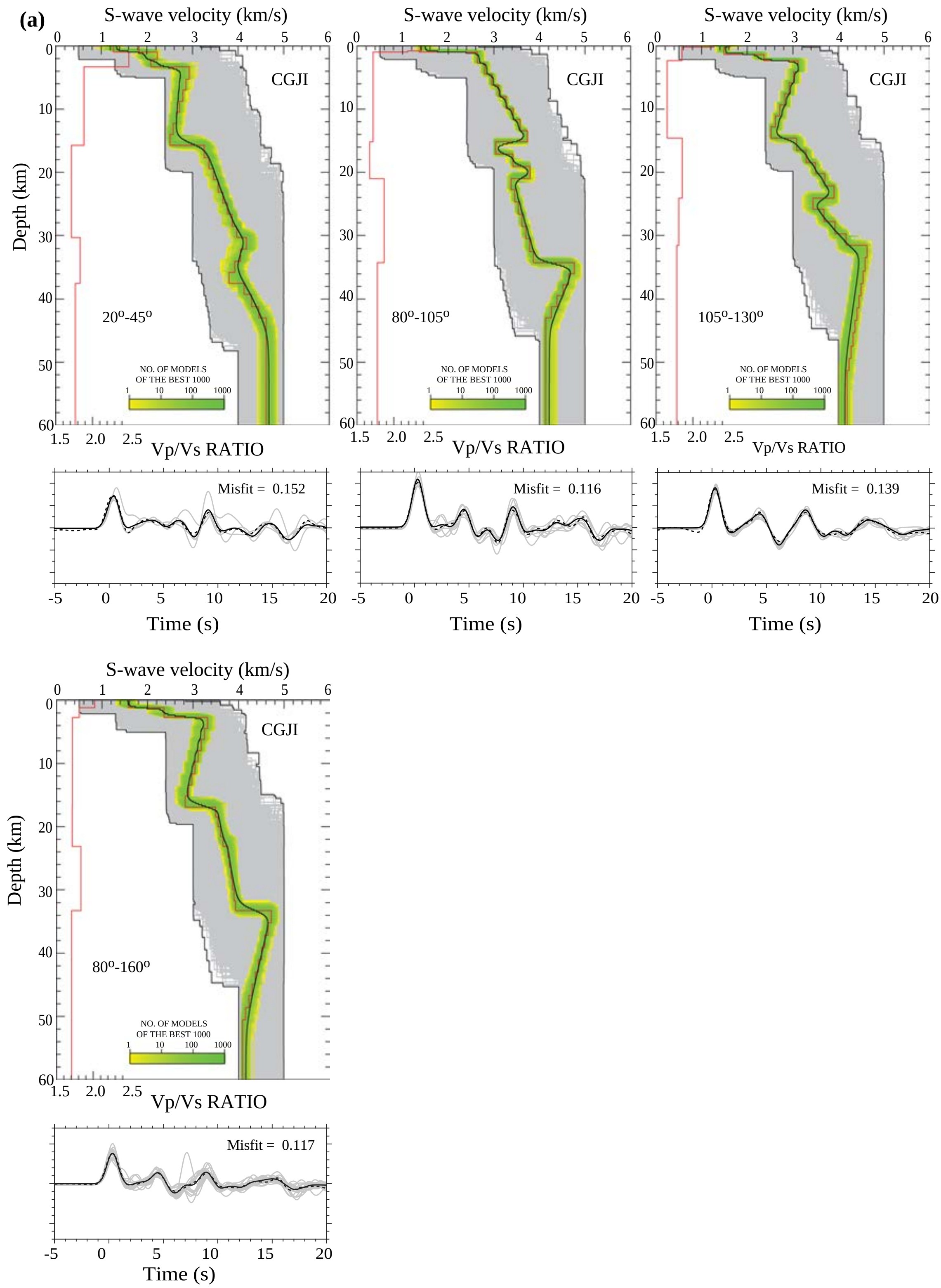

Figure 8. Derived *S*-wave velocity model for stations CGJI, CBJI, DBJI, and LEM located in Bogor-North Serayu-Kendeng Zone (upper panel). Lower panel shows calculated radial receiver functions (dashed line) using the best fitting *S*-wave velocity model from the nonlinear inversion, together with the observed stacked and individual radial receiver functions (solid black and grey lines). Details are same as figure 5.

surface and gradual increase of velocities in the crust. Transition between crustal and mantle velocities beneath CBJI station is estimated between 33 and 37 km depth. At station DBJI, stacked receiver function is limited in the back azimuth of 80°–105°. Inversion result shows

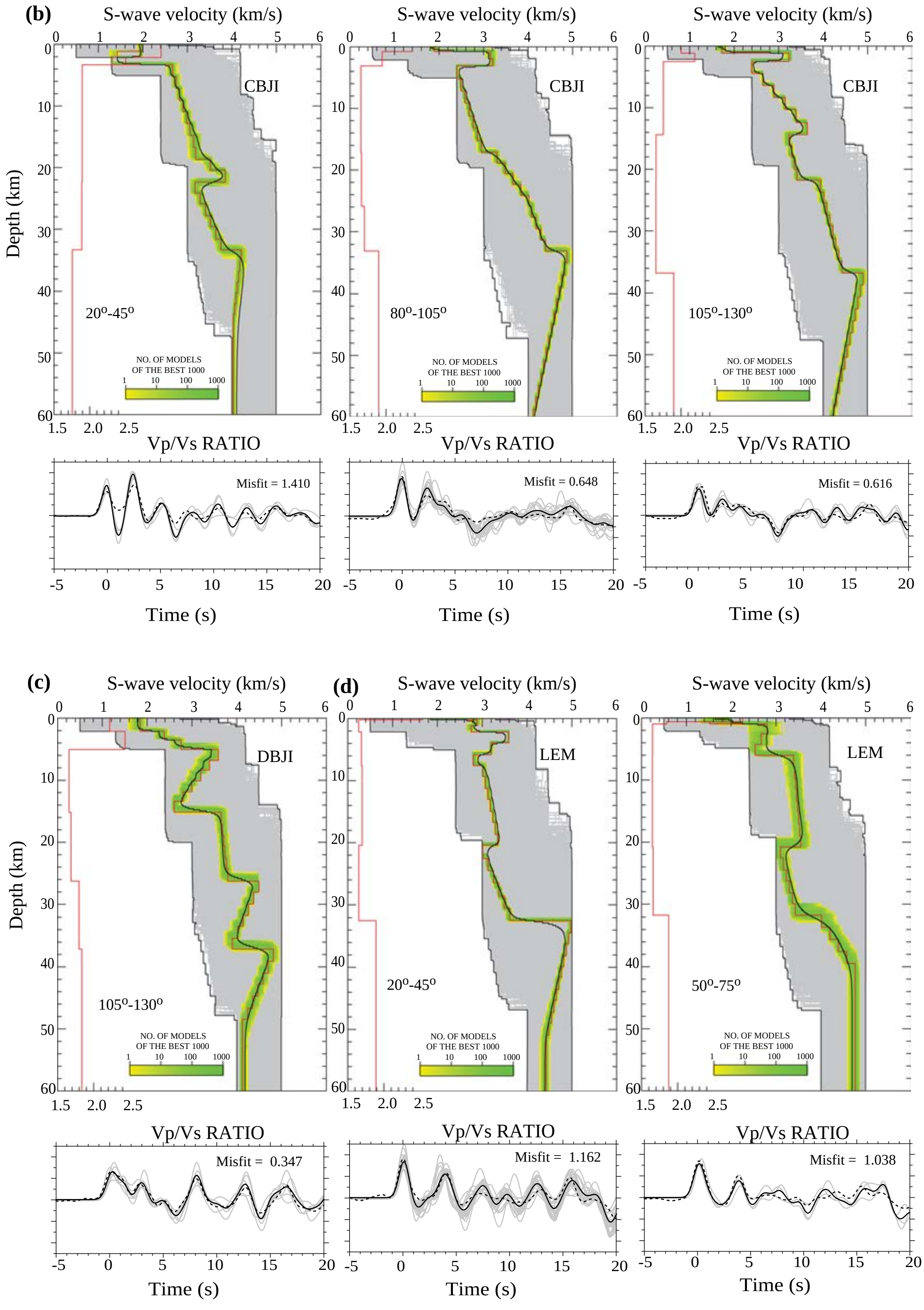

Figure 8. *(Continued.)*

varying crustal shear wave velocity. Crustal thickness, average crustal shear wave velocity Vs^c, and Vp/Vs^c beneath this station are estimated to be about 30 km, 3.63 km/s and 1.69, respectively. At station LEM, inversion of shear wave velocities are obtained from stacked receiver functions at five different back azimuths ranges. At back azimuths 20°–45° and 50°–75° show almost

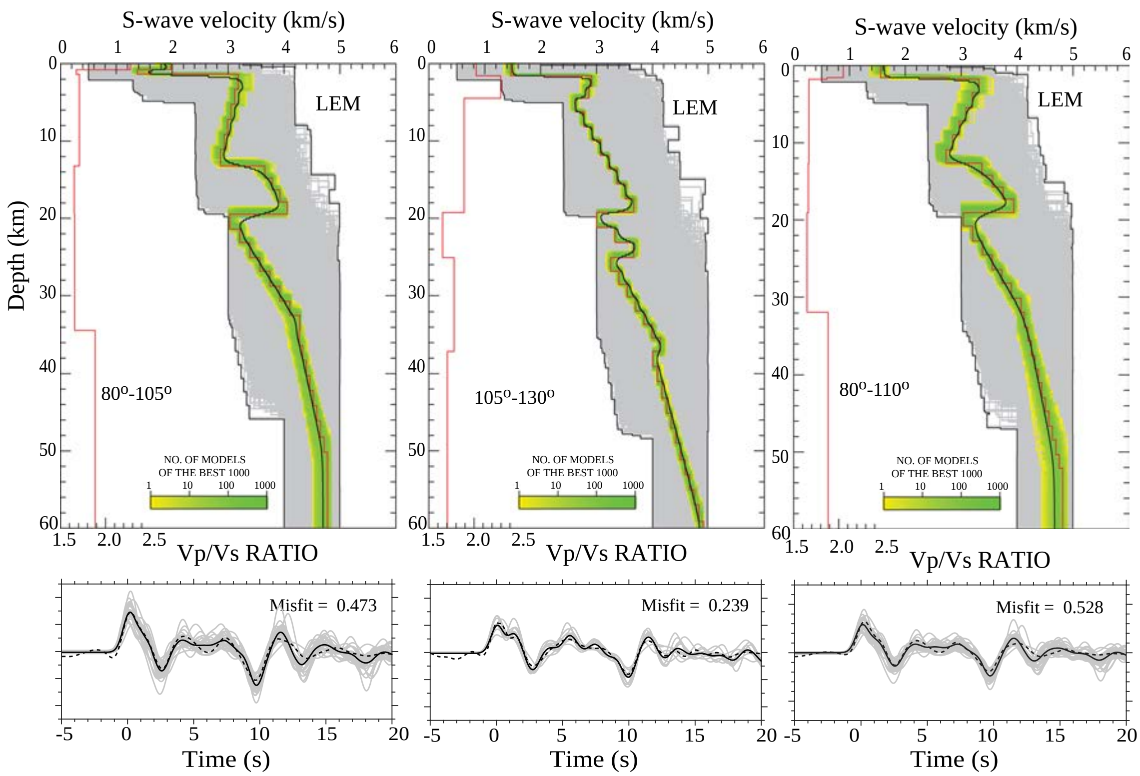

Figure 8. *(Continued.)*

similar characteristic of crustal shear wave velocity with gradual increase of the velocity down to depth of about 32 km indicating the Moho depth. At back azimuth 80°–105° we observe high velocity of about 3.8 km/s at depth of about 14–20 km, which is absent from other back azimuths. From the inversion result at this back azimuth, Moho layer is estimated at depth of about 34 km/s. At back azimuth 105°–130°, we observed gradual increase of crustal shear wave velocity to ~4.0 km/s indicating Moho layer at depth of about 37 km. At back azimuth 80°–110°, we observed similar characteristics of gradual increase of crustal velocity of about ~4.0 km/s indicating Moho Moho layer at depth of about 32 km. From inversion results of the stations in Bogor Zone, we suggest that the crustal thickness estimated to be in the range of 28–33 km thick. The estimated crustal Vp/Vs^c ratio in the Bogor Zone ranges between 1.65 and 1.90 (table 1).

Bogor Zone is part of Bogor-North Serayu-Kendeng Zone, which is a west–east trending anticlinorium. The anticlinorium extends from the western part of Java Island to the eastern part of Java Island and plunges beneath the alluvial plain in the Madura strait. van Bemmelen (1949) called this Bogor-North Serayu-Kendeng Zone as Central Depression. The Bogor Zone is characterized by anticlinorium of strongly folded Neogene strata with volcanic intrusion (e.g., van Bemmelen 1949; Satyana *et al.* 2002). Several studies suggested that Bogor-North Serayu-Kendeng Zone can be considered as deep portion of the basin in Java Island with sediment thickness up to several kilometers (e.g., van Bemmelen 1949; De Genevraye and Samuel 1972; Sujanto and Sumantri 1977). Western part of the Bogor Zone has a trend in the west–east direction; while in the eastern part it has a more WNW-ESE direction indicating a slightly convex to the North (Satyana *et al.* 2002). Using one temporary seismometer with location close to the LEM station, Hidayat *et al.* (2006) analysed receiver functions and suggested that sediment thickness beneath the station is about 1 km thick. They also suggested that the Moho depth is about 30–35 km, which is similar to our result from station LEM. A relatively large range of crustal Vp/Vs makes it difficult to discuss our results as no basement rocks exposed along Bogor-North Serayu-Kendeng Zone (e.g., Smyth *et al.* 2007).

4.3 *Southern mountains arc*

Observed receiver functions at station located in the Southern Mountains Arc are shown in figure 9.

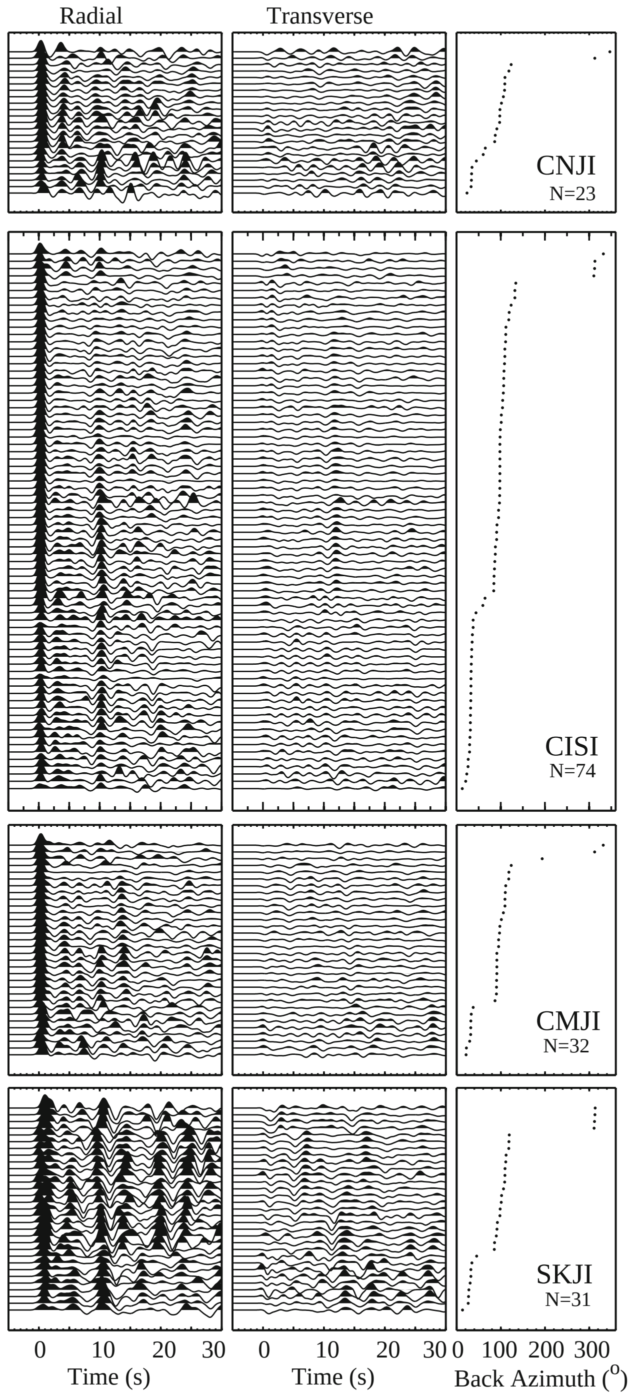

Figure 9. Observed receiver functions at stations located in Southern Mountains Arc.

Stations CNJI, CISI and CMJI show relatively similar characteristics of radial receiver functions. At station CNJI, direct *P* phase is generally observed at 0 s. However, at back azimuth of about 20° direct *P* phase shows a slight delay. Observed clear and strong direct *P* phase suggesting little effect of sedimentary layers to the receiver functions. *Ps* converted phase is estimated at 4–5 s. At station CISI, clear direct *P* phase is also generally observed at 0 s. For back azimuth of 20°, we observe a slightly change of direct *P* phase. *Ps* converted phase is estimated at 3–5 s. For back azimuth of 80°–140°, *Ps* converted phase is not clearly observed suggesting the presence of lateral heterogeneity beneath station CISI. At station CMJI, clear direct *P* phase is generally observed at 0 s. For back azimuth 20°, direct *P* phase is shown slight delay. *Ps* converted phase is generally found at 4–5 s. Complex receiver functions are observed at station SKJI suggesting the presence of complex heterogeneity beneath this station. The phases in the first two second may reflect the presence of low velocity layer near the surface beneath the station. This station is also located very close to the Cimandiri fault zone. This structural geology may also contribute to the complexity of the observed receiver functions (e.g., Zhang and Langston 1995; Savage 1998).

S-wave velocity profiles derived from the inversion for stations located in the Southern Mountains Arc are shown in figure 10. Crustal structure at station CNJI can be derived from stacked receiver functions from three different back azimuth ranges. At station CNJI, *S*-wave low velocity is observed down to about 1 km depth. At back azimuth range of 20°–45° and 80°–105° shows Moho layer is estimated at depth of about 25–26 km. At back azimuth ranges 105°–130° and 50°–130°, Moho layer is estimated at about ∼31 to 32 km depth (figure 10a). Crustal thickness, average crustal shear wave velocity Vs^c and Vp/Vs^c are estimated about 23–28 km, 3.62–3.76 km/s and 1.67–1.89, respectively. At station CISI, low velocity layers of 1 km thick with shear wave velocity of about 1.6 km/s are observed from inversion of receiver functions at four back azimuth ranges (figure 10b). Crustal thickness beneath this station ranges between 24 and 32 km with average crustal shear wave velocity varies between 3.29 and 3.89 km/s and Vp/Vs^c is estimated in the range of 1.69–1.86. Inversions of crustal structure for station CMJI are shown in figure 10(c). Low velocity layer thickness is estimated between 1 km thick (back azimuths 80°–105°, 105°–130° and 80°–130°) and 2 km thick (back azimuth 20°–45°). Crustal thickness, average crustal velocities Vs^c, and Vp/Vs^c are estimated about 30–34 km thick, 3.44–3.78, and 1.72–1.86, respectively. At station SKJI, low velocity layer varies between 1 and 2 km thick (figure 10d). At back azimuth range, shear wave velocity of about 2.6 km/s is observed at depth of ∼2 to 18 km which is absent from other back azimuths. The difference may suggest anisotropy or inhomogeneous medium beneath

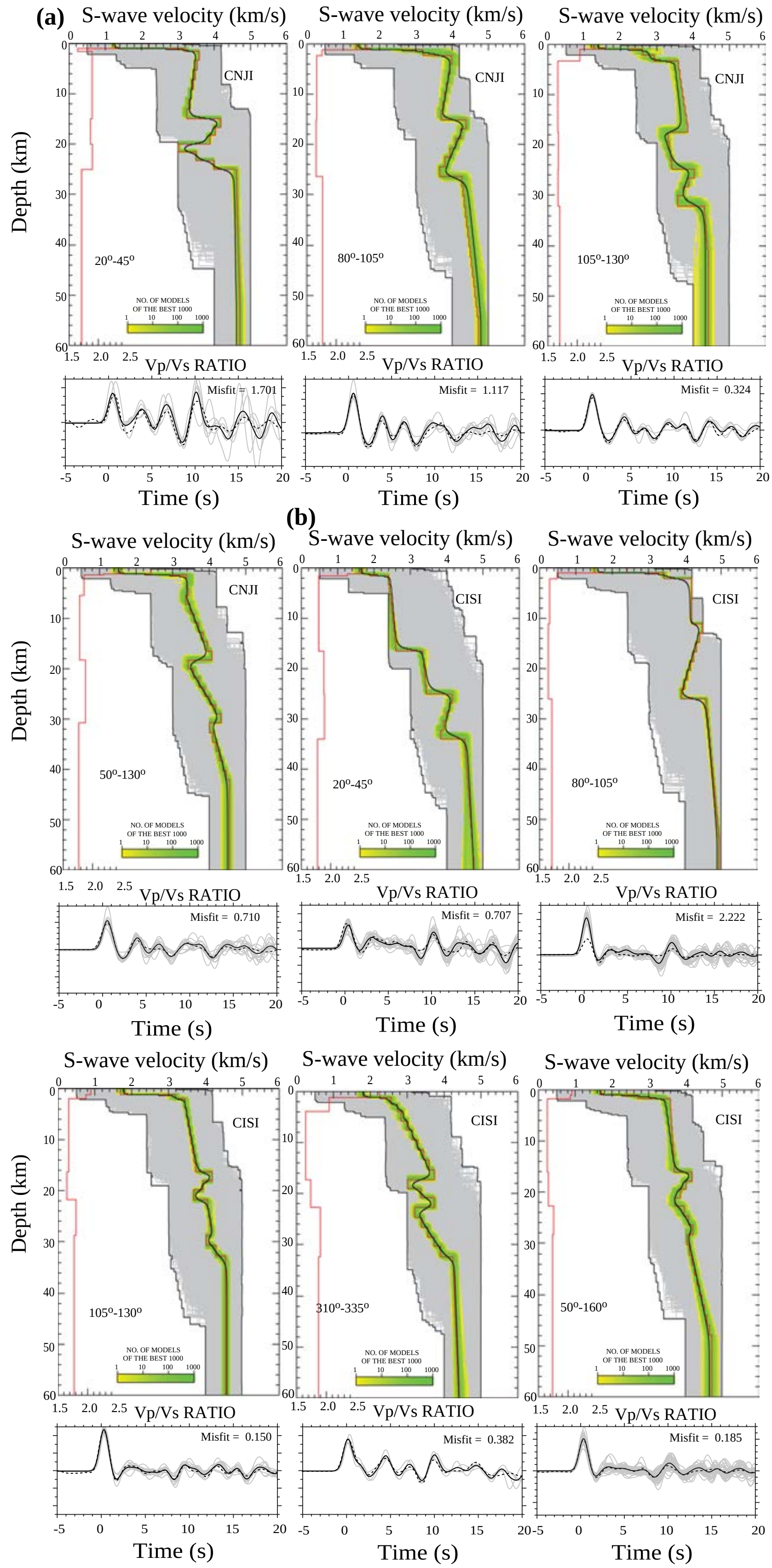

Figure 10. Derived *S*-wave velocity model for stations CNJI, CISI, CMJI and SKJI located in Oligocene-Miocene volcanic arc (upper panel). Lower panel shows calculated radial receiver functions (dashed line) using the best fitting *S*-wave velocity model from the nonlinear inversion, together with the observed stacked and individual radial receiver functions (solid black and grey lines). Details are same as figure 5.

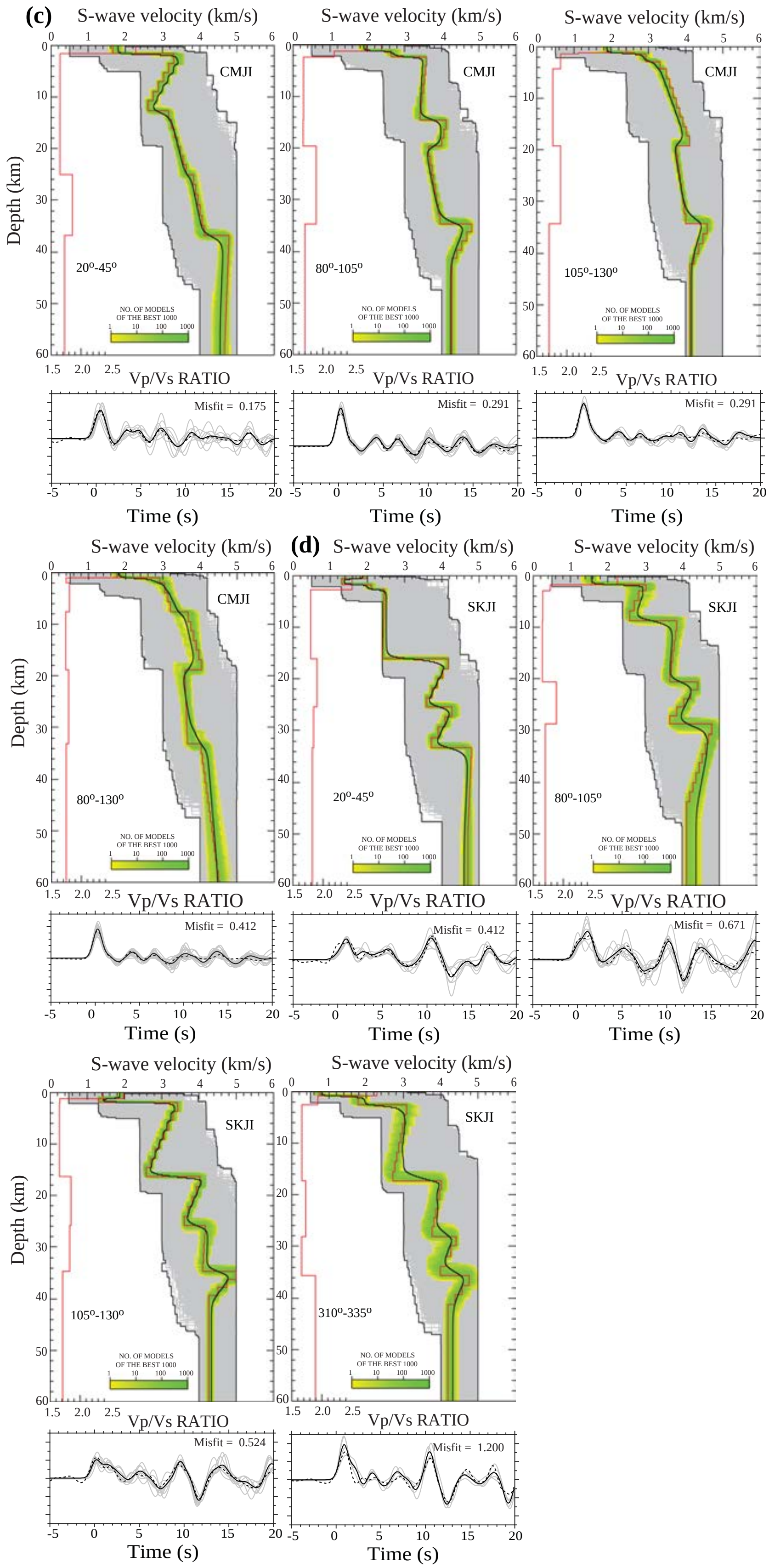

Figure 10. *(Continued.)*

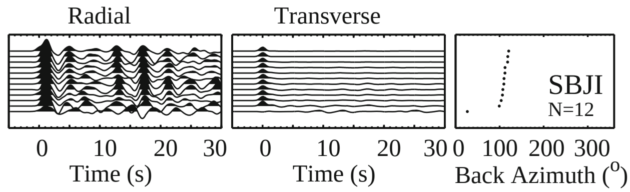

Figure 11. Observed receiver functions at station SBJI located on Quartenary deposit of Banten Tuff.

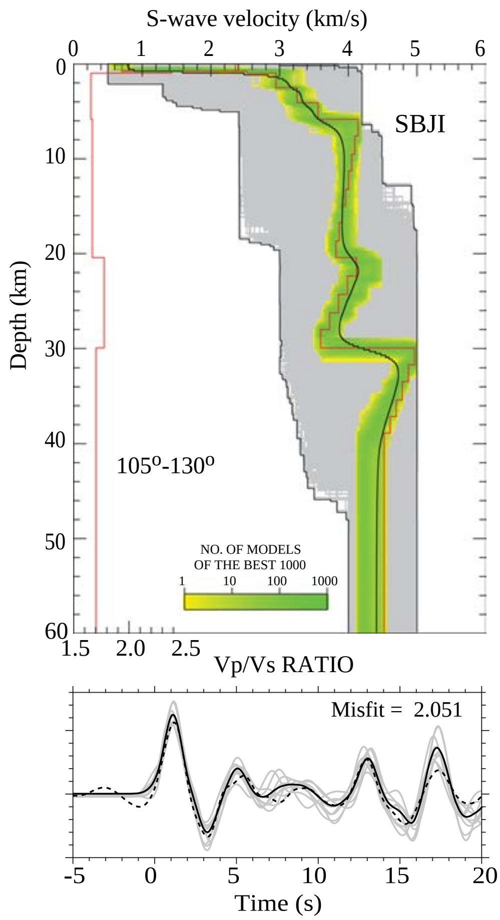

Figure 12. Derived *S*-wave velocity model for station SBJI located on quaternary deposit of Banten tuff (upper panel). Lower panel shows calculated radial receiver functions (dashed line) using the best fitting *S*-wave velocity model from the nonlinear inversion, together with the observed stacked and individual radial receiver functions (solid black and grey lines). Details are same as figure 5.

the station. At station SKJI, crustal thickness, average crustal shear wave velocity Vs^c, and Vp/Vs^c are estimated of 24–32 km, 3.38–3.61 km/s and 1.69–1.84, respectively. From receiver functions inversion at stations in the Southern Mountains Arc ranges, we estimated that Vp/Vs^c ranges between 1.67 and 1.89, the crustal thickness is estimated about 23–34 km thick and Vs^c of 3.29–3.85 km/s.

Few exposures of basement rocks in the Southern Mountains Arc are found in western Java. In Early Cretacious, subduction process occurred beneath Sunda block along Meratus suture which ran from Southwest Java to the Meratus mountains in Kalimantan (e.g., Wakita 2000; Clements and Hall 2007). These tectonic process resulted in arc volcanism, oceanic and forearc sedimentation, and metamorphism. In western Java, accretionary exposed rocks are found in Ciletuh and they include serpentinized peridotites, gabbros, pillow basalts and metamorphic rocks such as quartize and amphibolite (Clements and Hall 2007). Collision of continental fragment of Gondwana origin suggested to terminate subduction process, and part of this fragment might form part of basement in East Java (Smyth *et al.* 2007). Sedimentary rocks in the Southern Mountains Arc were deposited above the basement. Several studies have estimated that stratigraphic thickness in this arc may up to about 2.5 km thick, which is consistent with our observation from four stations ranging from 1 to 2 km (van Bemmelen 1949; Soeria-Atmadja *et al.* 1994). Crustal thickness in Southern Mountains Arc in western Java is estimated about up to about ∼37 km thick. Similar result is obtained by Wölbern and Rümpker (2016) carried out H-K stacking analysis of receiver functions from MERAMEX temporary network in Central and East Java. High Vp/Vs ratio in the lower crust of southwestern Japan is observed from seismic tomography, which might be related to the high pore-pressure resulting from fluid dehydration of Philippine oceanic crust (Matsubara *et al.* 2008). Other studies in subduction zone of Japan (Kodaira *et al.* 2004), Cascadia (Audet *et al.* 2009) and collision zone of Banda (Syuhada *et al.* 2016) showed high Vp/Vs ratio with low *S*-wave velocity.

4.4 *Quaternary deposit of Banten tuff*

Figure 11 shows receiver functions at station SBJI, located on quaternary deposit of Banten tuff (Rusmana *et al.* 1991). van Bemmelen (1949) suggested that volcanic activity in this area took place from the Late Pleistocene until Holocene, which is indicated by the formation of volcanoes in the area. Most of the events used to calculate receiver functions are limited within back azimuth of 20°–120°. Clear direct *P* phases are generally observed with slightly delayed around 0 s. For back azimuth of 20°–30°, direct *P* phase is slightly broadened suggesting the presence of low velocity layer beneath the station. *Ps* converted phases are estimated between 4 and 6 s. *S*-wave velocity profile from inversion of radial receiver functions is obtained at back azimuth range of 105°–130° (figure 12). The inversion solution shows a low *S*-wave velocity of about 1.0 km/s near surface down to 1 km indicating presence of sedimentary layer. *S*-wave velocity increases to about 3.8 km/s at depth of about 10 km. It then slightly fluctuates down to depth of about 30 km. The *S*-wave velocity increases to be about 4.3 km/s at depth of ~30 km. The crustal Vp/Vs^c ratio beneath this station is estimated to be 1.70. The station sits on top of Banten tuff, which is estimated to be Pleistocene age. Crustal thickness beneath station SBJI is consistent with the crustal thickness from the observation at stations located at Northwest Java basin (~32 km), which is considered part of Sunda block.

5. Conclusion

We estimated crustal structure in beneath seismic network in Western Java, Indonesia by inverting stacked teleseismic receiver functions using non-linear neighbourhood algorithm. We obtained that sediment thickness variations in this region is about 1–2 km. Crustal thickness and Vp/Vs ratios at stations located in the northern part of Western Java, which coincides with Northwest Java Basins and Quartenary Banten tuff, are estimated to be ~25 km and ~1.72 to –1.75, respectively. For stations located in Bogor Zone, crustal thickness and Vp/Vs ratio are estimated ~30 to 32 km and 1.69–1.77, respectively. At stations located in the Southern Mountains Arc, crustal thickness and Vp/Vs ratio are estimated ~25 to 32 km and 1.75–1.78, respectively. Relatively large variation of crustal thickness and Vp/Vs ratio in the Western Java could be suggested to the origin of tectonic block in this region, where west of Meratus suture is related to the Sunda block while the Southern Mountains Arc might be related to the Australian continental.

Acknowledgements

This study was supported by Indonesian Ministry of Research Technology and Higher Education through INSINAS No. 060/P/RPL-LIPI/INSINAS-1/III/2018. Seismic data were obtained from the GEOFON data centre of the GFZ German Research Centre for Geosciences. Some figures were prepared using Generic Mapping Tools (GMT) by Wessel and Smith (1991). We are very grateful for the comments from reviewers that improved the manuscript. Some of the figures were created using GMT.

References

Abidin H, Andreas H, Kato T, Ito T, Meilano I, Kimata F, Natawidjaja D and Harjono H 2009 Crustal deformation studies in Java, Indonesia using GPS; *J. Earthq. Tsunami* **3** 77–88.

Adnan A, Sukowitono and Supriyanto 1991 Jatibarang sub basin – a half graben model in the onshore of northwest Java; *Proc. 20th Annual Convention, Indonesian Petroleum Association,* pp. 279–297.

Ahmed A, Leroy S, Keir D, Korostelev F, Khanbari K, Rolandone F, Stuart G and Obrebski M 2014 Crustal structure of the Gulf of Aden southern margin: Evidence from receiver functions on Socotra Island (Yemen); *Tectonophys.* **637** 251–267.

Ammon C J, Randall G and Zandt G 1990 On the non-uniqueness of receiver function inversions; *J. Geophys. Res.* **95** 15303–15318.

Ammon C J 1991 The isolation of receiver effects from teleseismic P waveforms; *Bull. Seismol. Soc. Am.* **81** 2504–2510.

Audet P, Bostock M G, Christensen N I and Peacock S M 2009 Seismic evidence for overpressured subducted oceanic crust and megathrust fault sealing; *Nature* **457** 76–78.

Bai L, Tian X and Ritsema J 2010 Crustal structure beneath the Indochina peninsula from teleseismic receiver function; *Geophys. Res. Lett.* **37** L24308.

Bannister S, Yu J, Leitner B and Kennett B L N 2003 Variations in crustal structure across the transition from West to East Antarctica, Southern Victoria Land; *Geophys. J. Int.* **155** 870–884.

Bannister S, Bryan C J and Bibby H M 2004 Shear wave velocity variation across the Taupo Volcanic Zone, New Zealand, from receiver function inversion; *Geophys. J. Int.* **159** 291–310.

Bianchi I, Bokelmann G and Shiomi K 2015 Crustal anisotropy across northern Japan from receiver functions; *J. Geophys. Res.* **120** 4998–5012.

Bishop M G 2000 *Petroleum system of the Northwest Java Province, Java, and offshore Southeast Sumatra, Indonesia*; U.S. Geological Survey Open-File Report 99-50R.

Bora D K, Borah K and Goyal A 2016 Crustal shear-wave velocity structure beneath Sumatra from receiver function modeling; *J. Asian Earth Sci.* **121** 127–138.

Cassidy J F 1992 Numerical experiments in broadband receiver function analysis; *Bull. Seismol. Soc. Am.* **82** 1453–1474.

Chang S J and Baag C E 2005 Crustal structure in Southern Korea from joint analysis of teleseismic receiver functions and surface-wave dispersion; *Bull. Seismol. Soc. Am.* **95** 1516–1534.

Chevrot S and van der Hilst R D 2000 The Poisson ratio of the Australian crust: geological and geophysical implications; *Earth Planet. Sci. Lett.* **183** 121–132.

Christensen N I 1996 Poisson's ratio and crustal seismology; *J. Geophys. Res.* **101** 3139–3156.

Clements B and Hall R 2007 Cretaceous to late Miocene stratigraphic and tectonic evolution of West Java; *31st Indonesian Petroleum Association Annual Convention Proceeding* IPA07-G-037.

Clements B, Hall R, Smyth H R and Cottam M A 2009 Thrusting of a volcanic arc: A new structural model for Java; *Petrol. Geosci.* **15** 159–174.

Clements B and Hall R 2011 A record of continental collision and regional sediment flux for the Cretaceous and Palaeogene core of SE Asia: Implications for early Cenozoic palaeogeography; *J. Geol. Soc.* **168** 1187–1200.

Clitheroe G, Gudmundsson O and Kennett B L N 2000 Sedimentary and upper crustal structure of Australia from receiver functions; *Austr. J. Earth. Sci.* **47** 209–216.

Crotwell H P and Owens T J 2005 Automated receiver function processing; *Seismol. Res. Lett.* **76** 702–709.

Dardji N, Villemin T and Rampnoux J 1994 Paleostress and strike slip movement: The Cimandiri Fault Zone, West Java, Indonesia; *J. SE Asian Earth Sci.* **9** 3–11.

De Genevraye P and Samuel L 1972 Geologi of the Kendeng Zone (Central and East Java); *First Annual Indonesian Petroleum Association Proceeding,* pp. 17–30.

DeMets C, Gordon R G and Argus D F 2010 Geologically current plate motions; *Geophys. J. Int.* **181** 1–80.

Fountain D M and Christensen N I 1989 Composition of the continental crust and upper mantle: A review; In: Geophysical Framework of the Continental United States (eds) L C Pakiser Jr and Mooney W D, *Geol. Soc. Am. Memoir*, Boulder, Colorado, **172** 711–742.

Franke D, Schnabel M, Ladage S, Tappin D R, Neben S, Djajadihardja Y S, Muller C, Kopp H and Gaedicke C 2008 The great Sumatra–Andaman earthquakes-imaging the boundary between the ruptures of the great 2004 and 2005 earthquakes; *Earth Planet. Sci. Lett.* **269** 118–130.

Hall R 2012 Late Jurassic–Cenozoic reconstructions of the Indonesian region and the Indian Ocean; *Tectonophys.* **570–571** 1–41.

Hamilton W 1979 Tectonics of the Indonesian region; USGS Professional Paper 1078, 345p.

Harmon N, Henstock T, Tilmann F, Rietbrock A and Barton P 2012 Shear velocity structure across the Sumatran Forearc-Arc; *Geophys. J. Int.* **189** 1306–1314.

Hetényi G and Bus Z 2007 Shear wave velocity and crustal thickness in the Pannonian Basin from receiver function inversions at four permanent stations in Hungary; *J. Seismol.* **11** 405–414.

Hidayat D, Handayani L, Widiwijayanti C, Suyanto and Sanyoto 2006 Struktur lapisan bumi di bawah G. Tangkuban Perahu berdasarkan studi seismik stasiun tunggal (in Indonesian); *Riset-Geologi dan Pertambangan* **16** 1–8.

International Seismological Centre 2013 *On-line Bulletin*, Int. Seismol. Cent., Thatcham, United Kingdom, http://www.isc.ac.uk.

Kieling K, Roessler D and Krueger F 2011 Receiver function study in northern Sumatra and the Malaysian peninsula; *J. Seismol.* **15** 235–259.

Kodaira S, Iidaka T, Kato A, Park J O, Iwasaki T and Kaneda Y 2004 High pore fluid pressure may cause silent slip in the Nankai Trough; *Science* **304** 1295–1298.

Kopp H, Flueh E R, Klaeschen D, Bialas J and Reichert C 2001 Crustal structure of the central Sunda margin at the onset of oblique subduction; *Geophys. J. Int.* **147** 449–474.

Kopp H, Klaeschen D, Flueh E R, Bialas J and Reichert C 2002 Crustal structure of the Java margin from seismic wide-angle and multichannel reflection data; *J. Geophys. Res.* **107** 2034.

Kopp H, Hindle D, Klaeschen D, Oncken O, Reichert C and Scholl D 2009 Anatomy of the western Java plate interface from depth-mograted seismic images; *Earth Planet. Sci. Lett.* **288** 399–407.

Koulakov I, Bohm M, Asch A, Lühr B G, Manzanares A, Brotopuspito K S, Fauzi P, Purbawinata M A, Puspito N T, Ratdomopurbo A, Kopp H, Rabbel W and Shevkunova 2007 *P* and *S* velocity structure of the crust and the upper mantle beneath central Java from local tomography inversion; *J. Geophys. Res.* **112** B08310.

Koulakov I, Jakovlev A and Luehr B G 2009 Anisotropic structure beneath central Java from local earthquake tomography; *Geochem. Geophys. Geosyst.* **10** Q02011.

Langston C A 1979 Structure under Mount Rainier, Washington, inferred from teleseismic body waves; *J. Geophys. Res.* **84** 4749–4762.

Ligorria J P and Ammon C J 1999 Iterative deconvolution and receiver-function estimation; *Bull. Seismol. Soc. Am.* **89** 1395–1400.

Lodge A, Nippress S E J, Rietbrock A, García-Yeguas A and Ibáñez J M 2012 Evidence for magmatic underplating and partial melt beneath the Canary Islands derived using teleseismic receiver functions; *Phys. Earth Planet. Inter.* **212–213** 44–54.

Macpherson K A, Hidayat D and Goh S H 2012 Receiver function structure beneath four seismic stations in the Sumatra region; *J. Asian Earth Sci.* **46** 161–176.

Malod J A, Karta K, Beslier M O and Zen Jr M T 1995 From normal to oblique subduction: Tectonic relationships between Java and Sumatra; *J. SE Asian Earth Sci.* **12** 85–93.

Marliyani G I, Arrowsmith J R and Whipple K X 2016 Characterization of slow slip rate faults in humid areas: Cimandiri fault zone, Indonesia; *J. Geophys. Res. Earth Surf.* **121** 2287–2308.

Matsubara M, Obara K and Kasahara K 2008 Three-dimensional *P*- and *S*- wave velocity structure beneath the Japan Islands derived from the highdensity seismic stations by seismic tomography; *Tectonophys.* **454** 86–103.

Noble R A, Pratomo K H, Nugrahanto K, Ibrahim A M T, Prasetya I, Mujahidin N, Wu C H and Howes J V C 1997 Petroleum systems of Northwest Java, Indonesia; *Proc. International Conference on Petroleum Systems of SE Asia & Australasia,* pp. 585–600.

Park S J, Lee J M and Ryu I C 2009 1D velocity structure beneath broadband seismic stations in the Cretaceous Gyeongsang Basin of Korea by receiver function analyses; *Tectonophys.* **472** 158–168.

Parkinson C D, Miyazaki K, Wakita K, Barber A J and Carswell D A 1998 An overview and tectonic synthesis of the pre-Tertiary very-high-pressure metamorphic and associated rocks of Java, Sulawesi and Kalimantan, Indonesia; *Island Arc* **7** 184–200.

Patmosukismo S and Yahya I 1974 The basement configuration of the North West Java Area; *3rd Annual Indonesian Petroleum Association Convention Proceeding,* pp. 129–152.

Rusmana E, Suwitodirdjo K and Suharsono 1991 *Geological map of Serang quadrangle, Jawa;* Geological Research and Development Centre, Bandung, Indonesia.

Sambridge M 1999a Geophysical inversion with a neighbourhood algorithm – I. Searching a parameter space; *Geophys. J. Int.* **138** 479–494.

Sambridge M 1999b Geophysical inversion with a neighbourhood algorithm – II. Appraising the ensemble; *Geophys. J. Int.* **138** 727–746.

Satyana A H, Armandita C, Raharjo B and Syafri I 2002 New observation on the evolution of the Bogor Basin, West Java: Opportunities for turbidite hydrocarbon play; *Bull. Geologi Institut Teknologi Bandung,* pp. 1–15.

Savage M K 1998 Lower crustal anisotropy or dipping boundaries? Effects on receiver functions and a case study in New Zealand; *J. Geophys. Res.* **103** 15069–15087.

Saygin E, Cummins P R, Cipta A, Hawkins R, Pandhu R, Murjaya J, Masturyono, Irsyam M, Widiyantoro S and Kennett B L N 2016 Imaging architecture of the Jakarta Basin, Indonesia with transdimensional inversion of seismic noise; *Geophys. J. Int.* **204** 918–931.

Schlüter H U, Gaedicke C, Roeser H A, Schreckenberger B, Meyer H, Reichert C, Djajadiharja Y and Prexl A 2002 Tectonic features of the southern Sumatra-western Java forearc of Indonesia; *Tectonics* **21** 1047.

Sheehan A F, Abers G A, Jones C H and Lerner-Lam A L 1995 Crustal thickness variations across the Colorado Rocky Mountains from teleseismic receiver functions; *J. Geophys. Res.* **100** 20,391–20,404.

Shibutani T, Sambridge M and Kennett B L N 1996 Genetic algorithm inversion for receiver functions with application to crust and uppermost mantle structure beneath Eastern Australia; *Geophys. Res. Lett.* **23** 1829–1832.

Simons W J F, Socquet A, Vigny C, Ambrosius B A C, Abu S H, Promthong C, Subarya C, Sarsito D A, Matheussen S, Morgan P and Spakman W 2007, A decade of GPS in Southeast Asia: Resolving Sundaland motion and boundaries; *J. Geophys. Res.* **112** B06420.

Singh S C, Carton H, Tapponnier P, Hananto N D, Chauhan A P S, Hartoyo D, Bayly M, Moeljopranoto S, Bunting T, Christie P, Lubis H and Martin J 2008 Seismic evidence for broken oceanic crust in the 2004 Sumatra earthquake epicentral region; *Nat. Geosci.* **1** 777–781.

Smyth H R, Hamilton P J, Hall R and Kinny P D 2007 The deep crust beneath island arcs: Inherited zircons reveal a Gondwana fragment beneath East Java, Indonesia; *Earth Planet. Sci. Lett.* **258** 269–282.

Soeria-Atmadja R, Maury R C, Bellon H, Pringgoprawiro H, Polve M and Priadi B 1994 Tertiary magmatic belts in Java; *J. SE Asian Earth Sci.* **9** 13–17.

Sujanto F X and Sumantri Y R 1977 Preliminary study of the tertiary depositional patterns of Java; *6th Annual Indonesian Petroleum Association Convention Proceeding,* pp. 183–213.

Susilohadi S, Gaedicke C and Djajadihardja Y 2009 Structures and sedimentary deposition in the Sunda Strait, Indonesia; *Tectonophys.* **467** 55–71.

Suyitno P and Yahya I 1974 The basement configuration of the North West Java Area; *3rd Indonesian Petroleum Association Annual Convention Proceeding* 129–152.

van Bemmelen R W 1949 *The geology of Indonesia* Vol. 1 A, General geology of Indonesia and adjacent archipelagoes, The Hague, Matinus Nijhoff, Government Printing Office, 732p.

Wakita K 2000 Cretaceous accretionary–collision complexes in central Indonesia; *J. Asian Earth Sci.* **18** 739–749.

Wölbern I and Rümpker G 2016 Crustal thickness beneath Central and East Java (Indonesia) inferred from P receiver function; *J. Asian Earth Sci.* **115** 69–749.

Zandt G and Ammon C J 1995 Continental crust composition constrained by measurements of crustal Poisson's ratio; *Nature* **374** 152–154.

Zhang J and Langston C A 1995 Dipping structure under Dourbes, Belgium, determined by receiver function modeling and inversion; *Bull. Seismol. Soc. Am.* **85** 254–269.

Zhu L and Kanamori H 2000 Moho depth variation in southern California from teleseismic receiver functions; *J. Geophys. Res.* **105** 2969–2980.

Zulfakriza Z, Saygin E, Cummins P R, Widiyantoro S, Nugraha A D, Lühr B G and Bodin T 2014 Upper crustal structure of central Java, Indonesia, from transdimensional seismic ambient noise tomography; *Geophys. J. Int.* **197** 630–635.

Corresponding editor: Piyush Shanker Agram